SEISMIC PERFORMANCE OF BEAM-COLUMN JOINT REINFORCED WITH DIFFERENT SHAPE MEMORY ALLOY ALTERNATIVES

Kabir, Md Rashedul[1], Rizvi, Sosan[2], and Alam, M. Shahria[3,4]

[1] Graduate Student, School of Engineering, The University of British Columbia, Kelowna, BC, Canada
[2] Undergraduate Student, School of Engineering, The University of British Columbia, Kelowna, BC, Canada
[3] Associate Professor, School of Engineering, The University of British Columbia, Kelowna, BC, Canada
[4] shahria.alam@ubc.ca

Abstract: For seismic design based on the structural performance, to minimize the earthquake damage and possible seismic hazard scenarios to the structure, reinforcing the beam-column joints is crucial. Shape memory alloys are specially developed materials that exhibit the unique ability to return to their original shape after experiencing large stress deformations. Incorporation of SMA in the plastic hinge regions of beams of beam-column joints could potentially increase the ductility and reduce the residual deformation. Five various types of SMAs from the literature are being purposed as potential contenders in the SMA-Steel hybrid RC beam-column joint in this study. Numerical investigations of the beam-column joints have been carried out under reversed cyclic loading. The performance of the hybrid joints is scrutinized in terms of load-storey drift, energy dissipation capacity, and storey residual drift and compared to regular steel reinforced beam-column joint response. All the SMA-Steel hybrid beam-column joint proved to have adequate energy dissipation capacities with minimal residual storey drift under earthquake type loading.

1   Introduction

Structures in areas that experience high levels of seismic activity can often be subjected to earthquake damage from stress causing deformations and disturbing the integrity of the structure. Thus, reinforcing the weakest section of the structural system becomes vital, explaining the need to use materials with specific properties that can withstand permanent deformation for beam-column joints. Materials with more ductile properties are essential to avoid a collapsing structure that is encountering seismic stress. However, to make sure a repairable structure after a seismic event, reduced residual deformation needs to be ensured. Shape memory alloys (SMAs) are metal alloys that have unique properties such as superelastic (SE) and the shape memory effect. SMA as main reinforcement can recover inelastic deformation of structural elements at the end of tremors. SMAs are costly and impractical to use through an entire build, thus using at the critical regions like plastic hinge can mitigate problems with permanent deformations. Currently, in conventional seismic design of reinforced concrete (RC) structures, the steel reinforced bar is essentially supposed to absorb energy meeting the ductility demand. SMAs can be employed to improve the structural performance in seismic regions, structural integrity will be saved, fewer damage repairs will be needed, and overall economic efficiency will increase.

Shape memory alloys (SMAs) are metal alloys that have unique properties such as superelasticity (SE) and the shape memory effect. Focusing on SE SMA that possess the special property of returning to its original shape by stress removal after undergoing significant inelastic deformations, this characteristic gives SMAs the ability to enhance structural applications. Civil engineering application such as reinforcement in concrete structures, bolted joints, bracing, and isolators (Ocel et al. 2004). In particular structural application include

concrete prestressing (Maji and Negret 1998), bridge restrainers (Clark et al. 1995), and damping devices (Dolce et al. 2007, Andrawes and Desroches 2005). For instance, SMAs in steel beam-column joints were used to display repeated and stable hysteretic behavior (Ocel et al. 2004). SE SMA reinforced concrete beam-column joints can produce remarkable benefits in seismic regions due to their capability to dissipate significant amounts of energy with minimum rotation and deformation, supported by tests conducted by Saiidi and Wang (2006) and Youssef et al. (2008). Ni-Ti SMAs have an excellent non-corrosive property with great superelasticity. However, due to the high cost of Ni-Ti SMAs, Cu-based and Fe-based SMAs are gaining popularity (Dezfuli and Alam 2013, Czaderski et al. 2014).

This paper examines beam-column joints composed of five various types of SMAs which consist of Ni-Ti alloy, Cu-based and Fe-based alloys at the plastic hinge region of the beam to model SMA-Steel hybrid RC beam-column joints within this study. The performance of the hybrid joints is scrutinized in terms of load-storey drift, energy dissipation capacity and, residual storey drift and compared to regular steel reinforced beam-column joint response.

2   Research Significance

These different types of SMAs allow for the advancement of seismic design by increasing deformation capacity and ductility, higher damage tolerance, decreased residual crack size, and recovered or reduced permanent deformations (Billah and Alam 2016). Investigating SMAs of different compositions at the plastic hinge region when used within the application of beam-column joints will reveal how it changes the seismic impact on RC structures. The use of SMAs as reinforcement instead of steel in the plastic hinge locations of beams will absorb seismic energy efficiently and restore the original shape of members to some extent after seismic actions. The use of superelastic SMA as reinforcement instead of steel in the hinge locations of beams and columns is found promising in dissipating the seismic energy and in restoring the original shape of RC connection (beams-columns joints) after the seismic shocks (Alam et al. 2008). Before in field applications, RC connection must be investigated to predict their seismic performances. Structural engineers could use this novel material in designing RC connections with little damage and can minimize the post-earthquake damage repair cost. This paper discusses the behavior of various SMA-Steel hybrid RC beam-column joints during simulated seismic loading from the analytical point of view to give an insight on their comparative performance for future applications.

3   Shape Memory Alloy (SMA)

Shape memory alloys are smart materials that have distinct shape memory effect properties and superelasticity properties. Shape memory effect recovers the plastic strain upon heating, and superelasticity recovers the plastic strain once the load is removed; making SMA a unique material that can serve in replacement of conventional materials for numerous application in a wide range of engineering applications. Properties of these materials that are of extreme value are strong fatigue resistance and a high level of damping, transformation hysteresis responses, and resistance to corrosion, etc. These properties changes as the composition of the SMA changes. Ni-Ti alloys are the most used SMA due to its ability to recover from large strains, but their high cost limits its applications. Other various compositions that are composed of Fe-based and Cu-based are lower in cost and show excellent workability, machinability and wide transformation hysteresis in comparison to Ni-Ti alloys (Araki et al. 2010, Tanaka et al. 2010). In their rebar application in reinforced concrete structure at relatively high and low temperatures, Cu-Mn-Al bars maintain their superelastic behavior, thus allowing for this composition, in particular, to be suitable for use in the cold and warm region for seismic applications (Gencturk and Hosseini 2014). Several SMAs have been developed with various mechanical properties that result in different application ranges. In this study, five SMAs are considered, two Ni-Ti, two Fe-based and one Cu-based SMA. The mechanical properties of the SMAs are outlined in Table 1 (Billah and Alam 2016). These properties include elastic modulus, recovery strain, superelastic plateau strain length, and stress corresponding to the austenite and martensite stages.

Table 1: Properties of different types of SMAs

SMA type	Alloy	ε_s (%)	ε_r (%)	E (GPa)	f_y (MPa)	f_{p1} (MPa)	f_{T1} (MPa)	f_{T2} (MPa)	$\varepsilon_y=$ f_y/E	Reference
SMA-1	NiTi$_{45}$	6	0.5	62.5	401	510	370	130	0.0065	Alam et al. (2008)
SMA-2	NiTi$_{45}$	8	0.5	68	435	535	335	170	0.0064	Ghassemieh et al. (2012)
SMA-3	FeNCATB	13.5	1.5	46.9	750	1200	300	200	0.0159	Tanaka et al. (2010)
SMA-4	CuAlMn	9	0.4	28	210	275	200	150	0.0075	Shrestha et al. (2013)
SMA-5	FeMnAlNi	6.13	0.7	98.4	320	442.5	210.8	122	0.0033	Omori et al. (2011)

Note: f_y= austenite to martensite starting stress; f_{P1}= austenite to martensite finishing stress; f_{T1}= martensite to austenite starting stress; f_{T2}= martensite to austenite finishing stress, ε_s= superelastic plateau strain length; ε_r= recovery strain; and E= modulus of elasticity

4   Specimen Details

A beam-column joint specimen from Alam et al. (2008) is considered in this study to examine the performance of the structure replacing the reinforcement at the plastic hinge region of the beam. The control specimen is reinforced with regular steel only. All the specimens analyzed numerically are identical in geometry and dimensions, only the reinforcement configuration at the plastic hinge of the beam varies. The materials that are being investigated in this study are to be used to replace conventional steel, which is prone to corrosion and resulting in a damaged structure making it an unsustainable seismic resistant structures (Kabir et al. 2016). This is where SMAs can be applied to save the integrity of the structure due to its non-corrosive property and by allowing very little residual deformation at the weakest link in the structure, the beam-column joint. The exterior beam-column joint is isolated from an eight-story RC building with moment resisting frames at the points of contraflexure. The beam is taken to the mid-span of the bay, whereas the column is from the mid-column height of the fifth floor to the mid-column height of the sixth floor. Test specimen size is scaled down by 3/4, and the acting force on the joint was reduced by $(3/4)^2$ to maintain similar normal stress. Reduced axial force on the column of BCJ is taken 350 kN. Cross section of both the beam and column are 250 mm by 400 mm with longitudinal 4-M20 (diameter: 19.5 mm) steel. Transverse reinforcements in the column are spaced 80 mm in the joint region up to distance 500 mm above beam surface. For rest of the column length, the stirrup spacing is 115 mm. Similarly, ties in the beam are spaced 80 mm for 800 mm from column face (twice the depth of beam) and the rest of the part the spacing is 120 mm. The plastic hinge length is 360 mm from the face of the column. The material properties of the specimen are outlined in Figure 1 below, along with the geometric details.
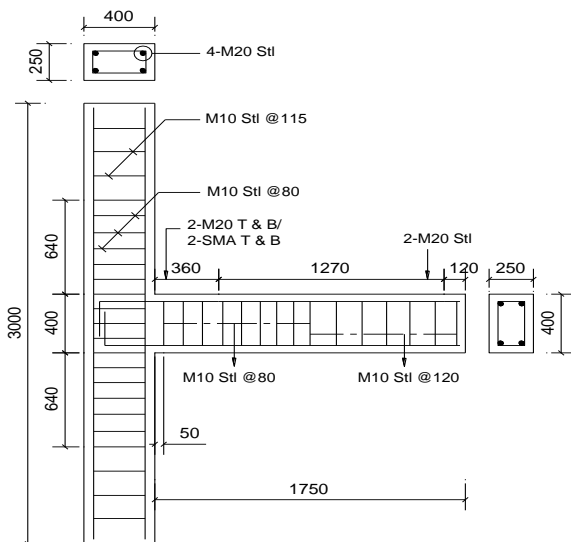
Concrete:
Compressive strength (MPa)   53.5
Split cylinder tensile strength (MPa)   3.5

Steel: (longitudinal)
Yield strength (MPa)   520
Ultimate strength (MPa)   630
Young's modulus (GPa)   198
Steel: (transverse)
Yield strength (MPa)   422
Ultimate strength (MPa)   682

Figure 1: Material properties of specimen and geometric details

Schematic illustrations of test setup and instrumentation of test specimens can be found in the original research (Alam et al. 2008). Load history for the reverse cyclic loadings is shown in Figure 2. A constant axial load of 350 kN is applied at the top of the column and reversed cyclic load applied at the beam tip. Tests were conducted up to a storey drift of at least 4%, which is more than the collapse limit (3%) defined by Kappos (1997), Kircil and Polat (2006). Loading applied at the beam tip was intended to induce high levels of deformations to depict the scenario of severe earthquake.
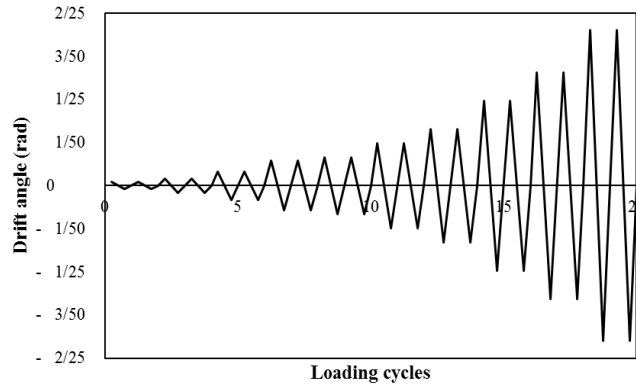
Figure 2: Loading protocol used for experiment

5   Finite Element Modelling

Finite Element (FE) simulation program SeismoStruct V7.0.4 (SeismoStruct 2015) is used to simulate and predict the displacement behavior of reinforced concrete structures under quasi-static loading considering both geometric nonlinearities and material inelasticity. The FE program can be applied to SMA material with a wide variety of pre-defined steel, concrete, and composite section configurations, and can create regular or irregular 2D/3D models. Figure 3 shows the model that is developed and used to run the analytical process. Several inelastic time history analyses have been carried out by the researchers to predict the performance of steel (Casarotti and Pinho 2006, Alam et al. 2008, Billah and Alam 2012, Billah and Alam 2013, Billah et al. 2017) and SMA (Alam et al. 2008, Billah and Alam 2016) reinforced concrete structural elements. The fiber modeling approach and 3D beam-column elements are used for modeling the beam and column joints (Figure 3) where the sectional stress–strain state of the elements is obtained through the integration of the nonlinear uniaxial stress–strain response of the individual fibers. Concrete has been modeled using the confinement concrete model proposed by Mander et al. (1998), and the concrete model does not account for tensile softening, and the concrete abruptly loses its tensile resistance as soon as the stress reaches its tensile strength (Alam et al., 2008). The constitutive laws of the reinforcing steel are considered from the model provided by Menegotto and Pinto (1973). SMAs are modeled according to the model of Auricchio and Sacco (1997). The beam-column joint is modeled using a 3D inelastic beam–column elements dividing it into a number of discrete segments as shown in Figure 3.
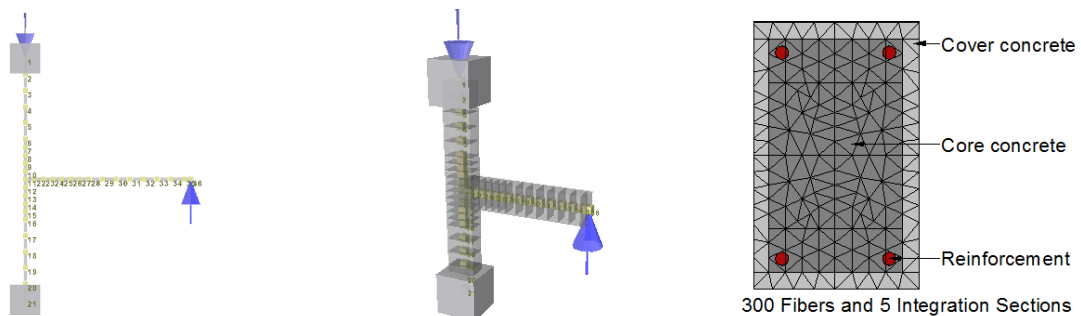

Figure 3: Finite element modeling of beam-column joint

Figure 4 illustrates the comparison between the experimental and numerical results and they are very similar to one another. The experimental data comparison indicates the FE model can predict large displacement behavior of structures. The beam tip load versus storey drift (%) plot shows the ultimate beam tip load is predicted as 60.04 kN at a storey drift of 3.96% compared to the experimental result of 65.5 kN at the same storey drift. The predicted maximum residual drift is found 2.23%, whereas the experimental value is 2.52%. The total predicted cumulative energy dissipation is 31.53 kN-m, which is only 6.5% lower than the corresponding experimental value (33.72 kN-m). In every case, predicted values are little lower than that of experimental results keeping the program outcomes on the safe side without overestimating the response. The numerical results show that the FE program is capable of predicting the force-displacement behavior of the joint with reasonable accuracy. The accuracy of the program in predicting the seismic response of bridge structures reinforced with SMA has been demonstrated by Billah and Alam (2016).
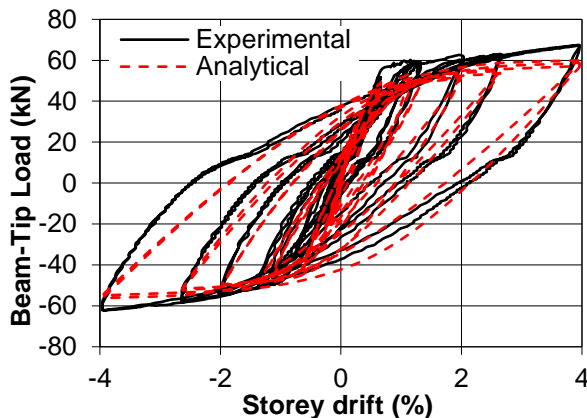

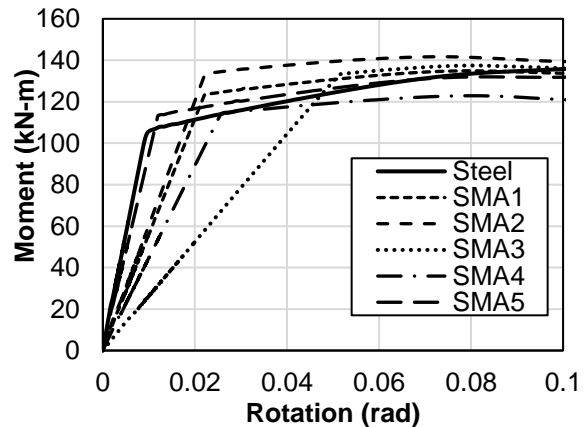Figure 4: Comparison with experimental result

Figure 5: Moment-rotation curve for different sections

SMAs display different stress-strain behavior than steel. The rebar size selected for SMAs are different from that of steel since they have different elastic modulus and yield strengths. Rebar sizes are chosen so that the axial forces on the rebar is similar (Araki et al. 2010). The relationship between the moment and rotation of the joint for all five SMAs and steel are analytically modeled, shown in Figure 5. Since the materials are of different elastic modulus and yield strength that is noted in Table 1, to have the moment capacity in the same range per rotation the diameters of the rebars from different compositions of SMAs vary from one another. The diameters are as following: SMA1 and SMA2 are 24mm, SMA3 is 18mm, SMA4 is 32mm and SMA5 is 26mm. Variation in the initial stiffness can be attributed to the different modulus of elasticity of the reinforcements. However, the maximum moment capacity of the control section is 135 kN-m whereas for SMAs, the minimum is 122.6 kN-m for SMA4 and the maximum is 141.6 kN-m for SMA2. 4-SE SMAs are used at the plastic hinge region of the beam as longitudinal reinforcement. Though the plastic hinge length is calculated 360 mm, the total length of 450 mm is considered for SMA bar to make provision for coupler in the joint. However, the effect of coupler is not considered in this study, perfect bonding between SMA and steel is considered. Previous work from Alam et al. (2008) showed that the program can predict the energy dissipation capacity with reasonable accuracy without bond slip consideration. Moreover, the bond slip behavior will be different for various types of SMA and steel combinations.

6   Results and Discussions

The beam tip load–storey drift relationship obtained from the FE analysis are described in this section along with the storey drift envelope, cumulative energy dissipation capacity and residual drift at the end cycles. Although the beam-column joint reinforced with different alternatives can undergo large deformation after yielding, to satisfy the life safety criterion found in FEMA 273 (1997), the inter-storey drift should be within the range 2%-2.5%. Collapse limit at 3% storey drift is presented in Kappos (1997), Kircil and Polat (2006), whereas Jeong and Elnashai (2007) considered 4% for collapse prevention of RC frame building. Performance parameters are compared mostly at 4% storey drift in this study. Lower residual drift with a

significant amount of energy dissipation capacity to reduce permanent deformation in the structure after a seismic event is also considered as a crucial criterion to recommend SMAs based on the FE analysis results for in-field structural applications.

6.1   Beam Tip Load vs. Storey Drift

Figure 6 illustrates story drift relationship with beam tip load of the models. Figures are compared up to 6% story drift. Steel, SMA1, and SMA2 do not allow storey drift more than 4% whereas SMA3, SMA4 and SMA5 can take 32% more storey drift. The ultimate beam tip load for the control beam-column joint is 67.5 kN at a drift ratio of 4%, whereas SMA1 specimen takes 74.4 kN of beam tip load at the same drift ratio. SMA2 specimen draws 1.34% higher load than that of SMA1 at similar storey drift. 70.9 kN, 69.3 kN and 72.6 kN beam tip load are carried out by SMA3, SMA4 and SMA5 correspondingly at 4% storey drift. However, these three SMAs have the capacity to undergo higher drift (more than 4%) before collapse (5.28%) at a reasonably high beam tip load (5.1% higher on an average) than that of steel.
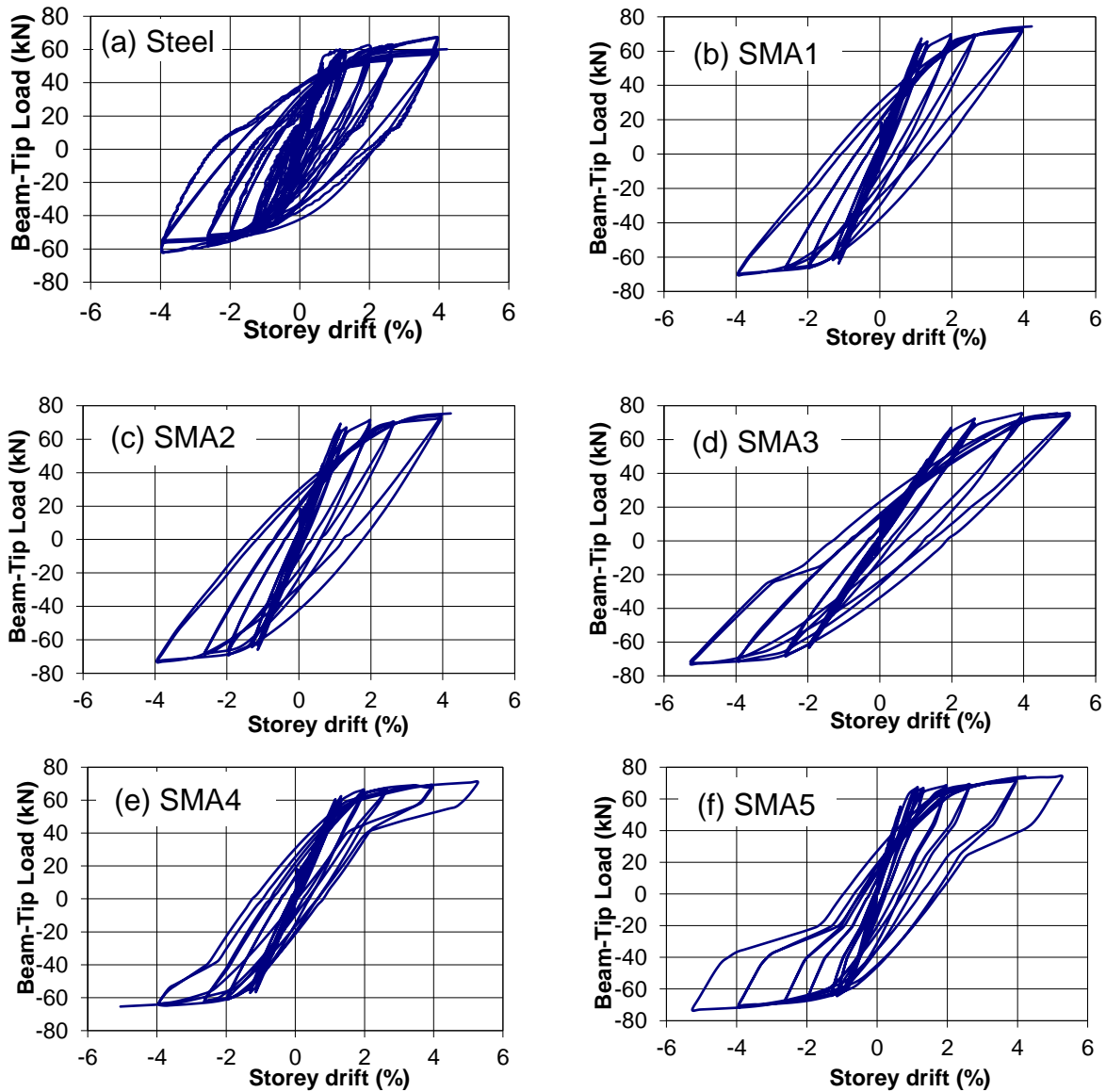
Figure 6: Beam tip load–storey drift relationship

EMM643-6

6.2   Beam Tip Load vs. Storey Drift Envelope

SMA3, SMA4, and SMA5 have almost the same load carrying capacity for the same percentage of storey drift (5.28%) while steel, SMA1, and SMA2 cannot go beyond 4% storey drift as can be seen from Figure 7. However, at the collapse drift limit of RC building, all types of SMAs take higher amount load (7.3% more) than that of conventional steel RC building. SMA3 and SMA4 display lower initial stiffness due to their lower modulus of elasticity, which might cause higher storey drift initially. This scenario changes after 2% storey drift and all the SMAs display same stiffness. The load-storey drift envelope plot clearly indicates the potential of SMA as longitudinal reinforcement in RC structural elements. Still, it cannot be the only deciding parameter since higher drift with lower energy dissipation capacity and high residual deformation will leave a structure unusable and ready to demolish.
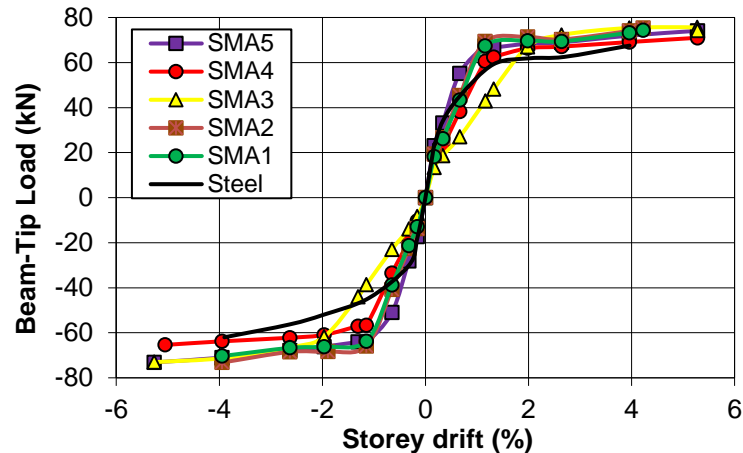

Figure 7: Beam tip load versus storey drift envelope

6.3   Cumulative Energy Dissipation Capacity vs. Storey Drift

The plot in Figure 8 represents the cumulative energy dissipation capacity versus storey drift for steel and the five SMAs. Energy dissipation capacity is determined from the area contained within the hysteresis loop in beam tip load-storey drift curve. The predicted maximum energy dissipation capacity is 33.7 kN-m, 25.8 kN-m & 24.2 kN-m for steel, SMA1 and SMA2 reinforced specimens respectively. With 1.42% higher value than steel, SMA5 shows the closest energy dissipation capacity to steel and the lowest being for SMA4 (20.8 kN-m). SMA3 displays 16% lower cumulative energy dissipation capacity than that of steel. At 4% storey drift, all types of SMAs exhibit lower energy dissipation capacity than that of steel. SMA3 displays the minimum capacity with 6.58 kN-m which is 80% less than steel cumulative energy dissipation capacity. Later on, it shows a sudden leap in energy dissipation capacity before failure. High superelastic plateau strain length and austenite to martensite starting stress can be attributed to this behavior.
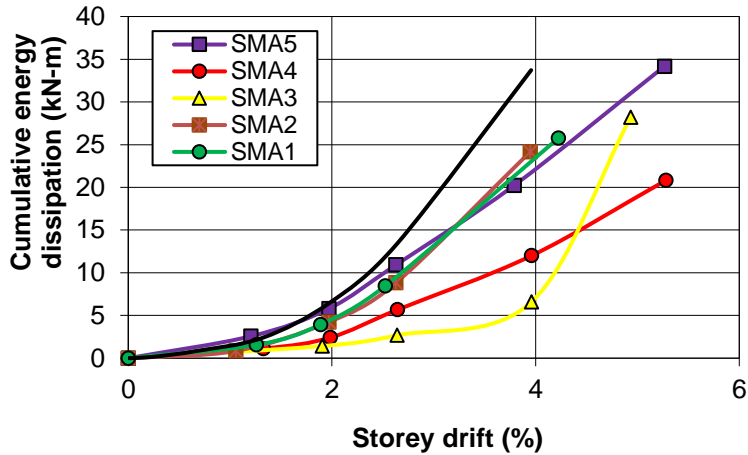
Figure 8: Cumulative energy dissipation-storey drifts relationship

6.4 Residual Drift vs. Load Cycle

The most significant property that makes SMA a potential candidate in structural engineering application is the superelasticity. Figure 9 demonstrates the residual storey drift at the end cycles of the beam-column joint models. Only the ends cycles are considered because, during the initial cycles, the residual drifts in the specimens are very little (less than 0.4%). The control specimen shows the maximum residual drift in every cycle and goes up to 2.47% maximum. All the specimens with SMA rebar at the plastic hinge region of beam reasonably reduce the residual storey drift. SMA4 is most effective among them. Maximum incurred residual drift by SMA4 it is 1.24%. SMA1, SMA2, SMA3 and SMA5 have almost similar recovery ability (1.56%, 1.78%, 1.85 and 1.74% respectively). However, after the 16th cycle, steel, SMA1, and SMA2 fail to take any more load. Up to 16th cycle, SMA3 shows more promising behavior in terms of recovering the initial position of the structure due to its high recovery strain (%).
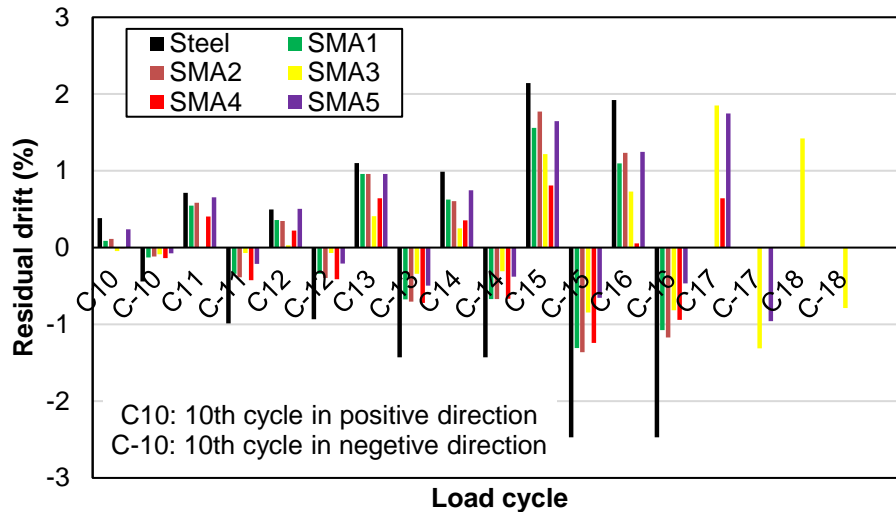

Figure 9: Residual drift at end load cycles

7 Conclusion

Seismic performance of a beam-column joint reinforced with different shape memory alloy alternatives at the plastic hinge location of the beam are assessed numerically, and the performances are compared to

EMM643-8

the control specimen reinforced with regular steel rebar. The performance of the hybrid joints is scrutinized regarding load-storey drift, cumulative energy dissipation capacity, and storey residual drift. All the SMA-Steel hybrid beam-column joint proved to have adequate energy dissipation capacities with minimal residual storey drift under simulated earthquake loading. The following conclusions can be drawn from this study.

- SMA-steel beam-column joint specimens displayed load-storey drift hysteresis similar to that of the steel with reduced stiffness and residual drift. Cu and Fe-based SMAs (SMA3, SMA4, and SM5) can take higher drift than Ni-Ti SMAs (SMA1 and SMA2). At 4% storey drift, all types of SMAs can take slightly higher amount of load than that of steel reinforced specimen (7.3% higher on an average). The load-storey drift envelope graph also signifies the potential of SMA as longitudinal reinforcement.

- Comparisons determine that the Fe-based SMA (Fe-Mn-Al-Ni), SMA5 provides the total maximum energy dissipation capacity of 34.2 kN-m with a storey drift of 5.27%, which is the maximum among the five SMAs which makes SMA5 very attractive in seismically active regions where the beam–column joints can dissipate significant amounts of energy. Ni-Ti SMAs are also capable of dissipating reasonably high amount of energy when introduced at the plastic hinge region.

- Shape memory alloy rebars show huge potential regarding the residual drift limitation. Before the collapse drift limit of RC buildings (4%), Fe-based (FeNCATB) SMA, SMA3 shows the best performance in reducing the residual drift in structure due to its higher high recovery strain property. Beam-column joint reinforced with SMA3 at the plastic hinge region underwent only 1.22% residual drift which is 50.6% less than that of the steel reinforced model. Other types of SMAs also showed satisfactory performance when compared to the control specimen.

The predicted results indicate that the five superelastic shape memory alloy can be used satisfactorily in the plastic hinge regions of beams of beam-column joints potentially increasing the ductility and reducing the residual deformation. This will lessen the probability of failure during seismic events and will keep the structure serviceable even after that. Fe and Cu based SMAs can be applied in structural engineering applications considering their lower price than Ni-Ti SMAs and satisfactory performances.

References

Alam, M., Youssef, M., and Nehdi, M. 2008. Analytical prediction of the seismic behaviour of superelastic shape memory alloy reinforced concrete elements. *Engineering Structures*, **30**(12): 3399-3411.

Andrawes, B., and Desroches, R. 2005. Unseating prevention for multiple frame bridges using superelastic devices. *Smart Materials and Structures*, **14**(3): S60–S67.

Applied Technology Council (ATC). 1997. *NEHRP Guidelines for Seismic Rehabilitation of Buildings*. Rep. No. FEMA 273, Prepared for the Building Seismic Safety Council (BSSC) by the ATC; Federal Emergency Management Agency: Washington, DC, USA.

Araki, Y., Endo, T., Omori, T., Sutou, Y., Koetaka, Y., Kainuma, R., and Ishida, K. 2010. Potential of superelastic Cu-Al-Mn alloy bars for seismic applications. *Earthquake Engineering & Structural Dynamics*, **40**(1): 107-115.

Auricchio, F., and Sacco, E., 1997. Superelastic shape-memory-alloy beam model. *Journal of Intelligent Material Systems and Structures*, **8**(6): 489–501.

Billah, A.H.M.M., and Alam, M.S. 2012. Seismic performance of concrete columns reinforced with hybrid shape memory alloy (SMA) and fiber reinforced polymer (FRP) bars. *Construction and Building Materials*, **28**(1), 730–742.

Billah, A.H.M.M., and Alam, M.S. 2013. Statistical distribution of seismic performance criteria of retrofitted multi-column bridge bents using incremental dynamic analysis: A case study. *Bulletin of Earthquake Engineering*, **11**(6), 2333–2362.

Billah, A.H.M.M., and Alam, M.S. 2016. Performance-Based Seismic Design of Shape Memory Alloy–Reinforced Concrete Bridge Piers. I: Development of Performance-Based Damage States. *Journal of Structural Engineering*, **142**(12), 04016140.

Billah, A.H.M.M, Kabir, M.R., and Alam, M.S. 2017. *Comparative Collapse Performance Assessment of Bridge Pier under Near-Fault and Long Duration Ground Motions*. 16th World Conference on Earthquake Engineering, 16WCEE 2017 Santiago Chile, January 9th to 13th. Paper No. 1315.

Casarotti, C., and Pinho, R. 2006. Seismic response of continuous span bridges through fibre-based finite element analysis. *Earthquake Engineering and Engineering Vibration*, **5**(1):119–131.

Clark, P.W., Aiken, I.D., Kelly, J.M., Higashino, M., and Krumme, R. 1995. Experimental and analytical studies of shape-memory alloy dampers for structural control. *The Proc. of SPIE*, **2445**: 241–51

Czaderski, C., Shahverdi, M., Brönnimann, R., Leinenbach, C., and Motavalli, M. 2014. Feasibility of iron-based shape memory alloy strips for prestressed strengthening of concrete structures. *Construction and Building Materials*, **56**: 94–105.

Dolce, M., Cardone, D., and Ponzo, F.C. 2007. Shaking-table tests on reinforced concrete frames with different isolation systems. *Earthquake Engineering & Structural Dynamics*, **36**(5): 573-596.

Dezfuli, F.H., and Alam, M.S. 2013. Shape memory alloy wirebased smart natural rubber bearing. *Smart Materials and Structures*, **22**(4): 45013–45029.

Ghassemieh, M., Mostafazadeh, M., and Sadeh, M.S. 2012. Seismic control of concrete shear wall using shape memory alloys. *Journal of Intelligent Material Systems and Structures*, **23**(5): 535-543.

Gencturk, B., and Hosseini, F. 2014. *Use of Cu-Based Superelastic Alloys for Innovative Design of Reinforced Concrete Columns*. 10th U.S. National Conference on Earthquake Engineering Frontiers of Earthquake Engineering. July 21-25. 10NCEE Anchorage, Alaska

Jeong, S.H., and Elnashai, A.S. 2007. Probabilistic fragility analysis parameterized by fundamental response quantities. *Engineering Structures*, **29**: 1238–1251

Ocel, J., Desroches, R., Leon, R.T., Hess, W.G., Krumme, R., Hayes, J.R., and Sweeney, S. 2004. Steel Beam-Column Connections Using Shape Memory Alloys. *Journal of Structural Engineering*, **130**(5), 732-740.

Omori, T., Ando, K., Okano, M., Xu, X., Tanaka, I., Ohnuma, R., Kainuma, K., and Ishida, K. 2011. Superelastic Effect in Polycrystalline Ferrous Alloys. *Science*, **333**(6038): 68-71.

Kabir, M. R., Alam, M.S., Said, A., and Ayad, A. 2016. Performance of Hybrid Reinforced Concrete Beam Column Joint: A Critical Review. *Fibers*, **4**,13.

Kappos, A.J. 1997. A Comparative Assessment Of R/c Structures Designed To The 1995 Eurocode 8 And The 1985 Ceb Seismic Code. *The Structural Design of Tall Buildings*, **6**(1): 59-83.

Kircil, M.S., and Polat, Z. 2006. Fragility analysis of mid-rise R/C frame buildings. *Engineering Structures*, **28**(9), 1335-1345.

Maji, A.K., and Negret, I. 1998. Smart prestressing with shape memory alloy. *Journal of Engineering Mechanics*, **124**(10): 1121–8.

Mander, J.B., Priestley, M.J.N. and Park, R. 1988. Theoretical stress–strain model for confined concrete. *Journal of Structural Engineering*, **114**(8): 1804–26.

Menegotto, M., and Pinto, P.E. 1973. *Method of analysis for cyclically loaded R.C. plane frames including changes in geometry and non-elastic behaviour of elements under combined normal force and bending*. Symposium on the Resistance and Ultimate Deformability of Structures Acted on by Well Defined Repeated Loads. International Association for Bridge and Structural Engineering, Zurich, Switzerland, 15-22.

Shrestha, K.C., Araki, Y., Nagae, T., Koetaka, Y., Suzuki, Y., Omori, T., and Ishida, K. 2013. Feasibility of Cu–Al–Mn superelastic alloy bars as reinforcement elements in concrete beams. *Smart Materials and Structures*, **22**(2), 025025.

Saiidi, M.S., and Wang, H. 2006. Exploratory study of seismic response of concrete columns with shape memory alloys reinforcement. *ACI Structural Journal*, **103**(3).

SeismoSoft, 2015. SeismoStruct - A computer program for static and dynamic nonlinear analysis of framed structures, V 7.0.4 [online], available from URL: www.seismosoft.com

Tanaka, Y., Himuro, Y., Kainuma, R., Sutou, Y., Omori, T., and Ishida, K. 2010. Ferrous Polycrystalline Shape-Memory Alloy Showing Huge Superelasticity. *Science*, **327**(5972), 1488-1490.

Youssef, M.A., Alam, M.S., and Nehdi, M. 2008. Experimental Investigation on the Seismic Behavior of Beam-Column Joints Reinforced with Superelastic Shape Memory Alloys. *Journal of Earthquake Engineering*, **12**(7): 1205-1222.